THE JOURNAL OF PHYSICAL CHEMISTRY B

pubs.acs.org/JPCB Article

Direct Observations of Silver Nanowire-Induced Frustrated Phagocytosis among NR8383 Lung Alveolar Macrophages

Evgeny Ogorodnik, Arpad Karsai, Kang-Hsin Wang, Fu-tong Liu, Su Hao Lo, Kent E. Pinkerton, Benjamin Gilbert, Dominik R. Haudenschild, and Gang-yu Liu*

Cite This: J. Phys. Chem. B 2020, 124, 11584–11592 Read Online

ACCESS | Metrics & More | Article Recommendations

ABSTRACT: The interaction of long nanowires and living cells is directly related to nanowires' nanotoxicity and health impacts. Interactions of silver nanowires (AgNWs) and macrophage cell lines (NR8383) were investigated using laser scanning confocal microscopy and single cell compression (SCC). With high-resolution imaging and mechanics measurement of individual cells, AgNW-induced frustrated phagocytosis was clearly captured in conjunction with structural and property changes of cells. While frustrated phagocytosis is known for long microwires and long carbon nanotubes, this work reports first direct observations of frustrated phagocytosis of AgNWs among living cells in situ. In the case of partial penetration of AgNWs into NR8383 cells, confocal imaging revealed actin participation at the entry sites, whose behavior differs from microwire-induced frustrated phagocytosis. The impacts of frustrated phagocytosis on the cellular membrane and cytoskeleton were also quantified by measuring the mechanical properties using SCC. Taken collectively, this study reveals the structural and property characteristics of nanowire-induced frustrated phagocytosis, which deepens our understanding of nanowire–cell interactions and nanocytotoxicity.

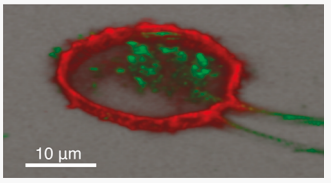

INTRODUCTION

Silver nanowires (AgNWs) represent an important class of engineered nanomaterials with a wide range of applications, including stretchable strain sensors,[1] flexible transparent touch panels,[2] wearable generators, organic light-emitting diodes (OLEDs),[3] and antimicrobial materials.[4] The rapid development of the nanotechnology industry[5] has raised concerns about potential acute and chronic health impacts following exposure, e.g., via inhalation,[6] ingestion, or skin contact.[7] Therefore, knowledge of macrophage–nanowire interactions represents an initial and critical step to understand and mitigate health impacts. From a fundamental research perspective, nanowires (NWs) in general, including AgNW specifically, have unique structural features including a high aspect ratio (length:width) and a nanometer scale diameter. These structural features generate important scientific questions, such as whether NWs exhibit cellular interactions and features of cytotoxicity different from those of micro- and macrowires[8] and nanoparticles.[9−11] Cytotoxicity has been observed in vitro for AgNWs,[12,13] with higher cytotoxicity caused by longer AgNWs.[13] In addition, in vivo studies have shown that high-aspect ratio AgNWs cause significantly greater pro-inflammatory response among macrophages than nanoparticles.[14,15] The long-term outcomes of exposure to AgNWs in the lung include severe, prolonged inflammation and tissue damage.[16] A natural and logical explanation extrapolated from interactions between cells and micro- and macrowires is frustrated phagocytosis (also known as incomplete phagocytosis) or the failure of macrophages to completely engulf the wires.[16] Frustrated phagocytosis is known to occur due to exposure to microfibers, such as asbestos[17] and microscale bundles of polymer nanofibers.[18] Given the structural features of AgNWs, similar fundamental questions arise: whether frustrated phagocytosis could also be induced by nanowires, and if so, would there be a difference from currently known frustrated phagocytosis, e.g., caused by microfibers.

Scanning electron microscopy (SEM) and bright field optical microscopy have been used to view cell–AgNW systems. These prior studies have pointed out AgNW-induced frustrated phagocytosis among macrophages,[16,19] since SEM images clearly demonstrate partially internalized wires. While informative, there remains the standing question of whether partially internalized nanowires occur while cells are alive and functioning, since sample preparation for SEM imaging requires cellular fixation, drying, and an ultrahigh vacuum (UHV) environment. Bright field imaging enabled imaging of living cells;[19] however, it faces the challenge of lacking 3D information, leading to uncertainty about the nanowire location with respect to the cell (inside versus above or underneath the cell).

Received: September 6, 2020
Revised: November 23, 2020
Published: December 11, 2020

https://dx.doi.org/10.1021/acs.jpcb.0c08132
J. Phys. Chem. B 2020, 124, 11584–11592

In contrast, atomic force microscopy (AFM) in association with scanning laser confocal microscopy (LSCM) can be utilized to monitor nanomaterial−cell interactions in situ and in 3D, while keeping cells viable in culture media.[9,20,21] Confocal imaging provides direct visualization of nanomaterials, cells, and intracellular structures and allows for determination of the precise location of the nanomaterial within the cell, while AFM enables measurements of cellular mechanics at a single cell level.[9,20,21] Prior studies also suggest nanomaterial uptake varies from cell to cell,[9] thus demonstrating that single cell-based technology is critical in documenting the actual interactions and in capturing frustrated phagocytosis. Using a macrophage cell line (NR8383), we carried out confocal imaging and single cell mechanics studies of cell−AgNW interactions in situ and in culture media. NR8338 is a rat alveolar macrophage cell line able to demonstrate active phagocytosis and killing in vitro. Therefore, NR8338 cells represent a good model of in situ alveolar macrophages to investigate nanomaterial−cell interactions in vitro, especially in the context of inhalation exposure and nanocytotoxicity.[22−28] Polyvinylpyrrolidone (PVP)-coated AgNWs have been previously used to investigate in vivo toxicity in rat lungs where acute and chronic inflammation was observed.[14] This study focuses on high-resolution in situ imaging with laser scanning confocal microscopy to observe frustrated phagocytosis of AgNWs directly during interactions with living NR8383 cells. In addition, the role of actin reorganization associated with frustrated phagocytosis was also demonstrated, taking advantage of the high spatial resolution. Single cell mechanics were also measured in association with the phagocytotic processes to test changes in the structural integrity of the cell membrane and actin cortex. Our findings reveal new insights into AgNW−macrophage interactions, especially in the context of frustrated phagocytosis. The approach and findings are of generic importance in the field of nanowire production and applications, nanowire−cell interactions, as well as cytotoxicity of nanowires.

METHODS

Materials. The *Rattus norvegicus* alveolar macrophage NR8383 [AgC11x3A, NR8383.1](ATCCCRL 2192) cell line was purchased from American Type Culture Collection (ATCC, Manassas, VA, U.S.A.). MatTek glass bottom dishes, P50G-1.5-30-F, were purchased from MatTek Corporation (Ashland, MA, U.S.A.). Mica sheets (clear ruby muscovite) were purchased from Ted Pella (Redding, CA, U.S.A.). Polished silicon wafers, Si(111) doped with boron, were purchased from Virginia Semiconductor Inc. (Fredericksburg, VA, U.S.A.). Poly-L-lysine (0.1% w/v, MW 150−300 kDa) was purchased from Sigma (St. Louis, MO, U.S.A.) and used without further purification. Deionized and ultrapure water was attained from a Milli-Q water system (EMD Millipore, Billerica, MA, U.S.A.). The following materials were purchased from Thermo Fischer Scientific (Waltham, MA, U.S.A.): 6-well plates, 75 cm^2 culture flasks, Ham's F12K medium containing 2 mM L-glutamine, 15% fetal bovine serum (FBS), penicillin/streptomycin solution (1.0×10^4 μg/mL each), 1X phosphate-buffered saline (PBS), and glass beads, 42.3 ± 1.1 μm in diameter. A ready-to-use pCMVLifeAct-TagRFP plasmid was purchased from ibidi, inc. (Madison, WI, U.S.A.). 1X Tris EDTA (TE) buffer, DNA condensation buffer (buffer EC), Enhancer and Effectene transfection reagents were purchased from Qiagen (Germantown, MD, U.S.A.) as parts of a kit. Two-component epoxy (S-31) was purchased from ITW performance polymers (Riviera Beach, FL). AFM cantilevers (AC 240) were purchased from Olympus America (Center Valley, PA). G418 antibiotic solution was purchased from Sigma (St. Louis, MO, U.S.A.). CO_2 was purchased from Airgas (Radnor, PA, U.S.A.). Polyvinylpyrrolidone (PVP)-coated AgNWs (Nanocomposix, Inc. San Diego, CA, U.S.A.) were supplied by the National Institute of Environmental Health Sciences Centers for Nanotechnology Health Implications Research (NCNHIR) consortium. Each solution consisted of 1 mg/mL AgNWs in ultrapure water. This solution was diluted with ultrapure water to reach a concentration of 100 μg/mL. Designated volumes of this solution were added to cell cultures to attain the designated AgNW concentrations, i.e., 1 and 10 μg/mL.

Preparation of NR8383 Cells. Handling, culturing, and maintenance of NR8383 cells follow the ATCC protocols.[29] Briefly, upon receipt, the cells were thawed by gentle agitation in a 37 °C water bath; then, the contents were transferred to a centrifuge tube containing 9.0 mL of complete culture medium (described below) and spun at 125 × g for 7 min. The cell pellet was resuspended and cultured in a 75 cm^2 culture flask in the 37 °C and 5% CO_2 incubator (Napco Series 8000 WJ CO_2 incubator, Thermo Electron, MA, U.S.A.). The complete culture medium was prepared by adding 15% fetal bovine serum (FBS) and 0.5% of penicillin/streptomycin solution (1.0×10^4 μg/mL each) to Ham's F12K (Kaighn's) medium containing 2 mM L-glutamine. Cells remained in the incubator for at least 3 days before exposure to designated concentrations of AgNWs or being subject to transfection. For AgNW exposure experiments, all cells were cultured in glass-bottom MatTek dishes.

Transfection of NR8383 Cells. For visualization of the actin cytoskeleton inside living cells in real time, a fluorescent cell line, NR8383-RFP, was produced by transfecting NR8383 cells with a red fluorescent protein (RFP)-bound actin tag. The plasmid contains an F-actin tag and a neomycin resistance gene. The Effectene transfection reagent was used for the transfection in accordance with the Effectene transfection handbook.[30] Briefly, $0.9-4 \times 10^5$ cells were seeded in each well of a 6-well plate with 1.6 mL of F12K medium and incubated overnight at 37 °C and 5% CO_2. The next day, 0.4 μg of plasmid DNA dissolved in TE buffer was added to 100 mL of buffer EC and then mixed with 3.2 μL of Enhancer. This mixture (transfection mixture) was incubated at room temperature for 5 min and centrifuged briefly. The Effectene transfection reagent (10 μL) then was added to the mixture and mixed by pipetting up and down and then allowed to mix for 10 min at room temperature. The media was aspirated from each well; then, the wells were washed with 3 mL of 1X PBS and 1.6 mL of a fresh growth medium. Next, 600 mL of the growth medium was added to the transfection mixture, mixed by pipetting up and down, and immediately added dropwise to the cell-containing wells. From this point on, the transfected cells were grown in the complete growth medium (F12K medium) with an additional 0.5% of G418 antibiotic solution (Sigma, St. Louis, MO, U.S.A.) at 37 °C and 5% CO_2.

Characterization of AgNWs Using Atomic Force Microscopy. AFM characterization was performed using the MFP-3D AFM (Asylum Research, Santa Barbara, CA). Microfabricated cantilevers (AC 240, Olympus America, Center Valley, PA) were employed for imaging. The mica (0001) surfaces were prepared by freshly cleaving mica then

https://dx.doi.org/10.1021/acs.jpcb.0c08132
J. Phys. Chem. B 2020, 124, 11584−11592

coating the surface with PLL by adding 30 μL of the PLL solution on top of the mica surface and letting it soak for 5 min. The surface was washed with ultrapure water and allowed to air dry in a laminar flow hood. For structure characterization of AgNWs, a 5 μL AgNW suspension (1 mg/mL) was placed on the PLL/mica (0001) surface and allowed to soak for 20 min. The surface was washed using ultrapure water and air dried in a laminar flow hood. The tapping mode was utilized to image these AgNW samples under ambient conditions. Typical driving frequency was set to the natural resonance frequency of the AFM cantilever (75 kHz). Free amplitude of the cantilever was set to 1 V, and a set point of 0.58 V was used. The scan rate was set to 0.80 Hz.

High-Resolution Imaging via Laser Scanning Confocal Microscopy. A laser scanning confocal microscope (FV-1000, Olympus America, Center Valley, PA) was utilized for visualizing and monitoring the AgNW−cell interactions. Unless specified, 60X bright field objective was used. Argon (458 nm) and HeNe (543 nm) lasers were utilized for excitation. For the photoluminescence spectrum determination, AgNWs were immobilized on a PLL-coated glass slide, following the procedure described above, while substituting glass for mica and omitting the cleaving step. Lambda scans of AgNWs were performed using a 458 nm excitation with a 4 nm step and 2 nm overlap between steps. For NR8383-RFP with AgNW imaging, the 458 nm excitation and 500−520 nm emission window were used for the AgNW channel, while the 543 nm excitation and 595−665 nm emission window were used for the NR8383-RFP channel. Most images are 640 × 640 resolution. For AgNW uptake measurements, 3D stacks of confocal images of NR8383 cells were analyzed using ImageJ. All images were taken with identical settings, e.g., focus, intensity, and sensitivity of the detector. The stacks covered the full height of the cell, at 0.5 μm increment. The images were taken at a 4 μs/pixel scanning speed. Using ImageJ, integrated density and the area of each cell were measured, as well as the mean background readings. Corrected total cell fluorescence (CTCF) was calculated using the following formula: CTCF = integrated density − (area of selected cell × mean fluorescence of background readings).[31]

Exposure of Cells to AgNWs. NR8383 cells were exposed to the designated concentrations of AgNWs (1 and 10 μg/mL) in culture media in the incubator for 24 h, at which point the media was exchanged with fresh media to remove free-floating AgNWs. One hour thereafter, the cells were imaged using combined bright field and confocal microscopy, and any wire that was observed to cross the cell boundary was considered a case of frustrated phagocytosis. Doing this after a 24 h exposure provided a better end-point for frustrated phagocytosis determination than other in vitro studies reported in the literature, which make that determination 4 h after exposure.[19]

Scanning Electron Microscopy Imaging and Energy Dispersive Spectroscopy. Polished silicon (111) was coated with PLL by adding 30 μL of the PLL solution on top of the silicon surface and allowed to soak for 5 min and then washed with ultrapure water then let dry. Subsequently, 5 μL of the AgNW suspension (1 mg/mL) was placed on the PLL/Si surface and allowed to soak for 20 min. Washing with ultrapure water followed, and the surfaces were allowed to dry. All SEM images were acquired using a field emission scanning electron microscope (FE-SEM) (Hitachi S-4100 T, Hitachi HTA, CA, U.S.A.) at an accelerating voltage of 10 kV. An energy dispersive spectrometer (EDS) (EDS Inca System, Oxford INCA Energy, MA, U.S.A.) was utilized to determine the chemical compositions and oxidation state of AgNWs.

Single Cell Mechanics Measurements. Single cell mechanics measurements were taken using an AFM-based method known as single cell compression (SCC). This method was developed by our team and was utilized to probe the mechanical properties of living cells in culture media.[9,20,21,32] Briefly, a 40 μm-diameter glass bead was glued to the end of an AFM cantilever using two-component epoxy. The cantilever's spring constant was determined by measuring its resonance frequency before and after glass bead attachment, then applying the added mass method[33] in conjunction with bead position correction.[34] Force deformation was first acquired at the bare glass surface next to the chosen cell to determine optical lever sensitivity and to establish the position of the surface. Then, the sphere was moved directly above the center of the cell, as guided by the inverted microscope (60X bright field objective). The cell compressions were performed at a relatively slow speed of 2 μm/s to avoid hydrodynamic impact.[20] Force-deformation profiles were displayed as force versus relative deformation, defined as a change in cell height over the height of the uncompressed cell. In order to quantify the elastic compliance for the cellular membrane and the cytoskeleton, Hertzian contact mechanics were adopted with the assumption that living cells behave like balloons containing fluid.[9,20,21] Assuming little attachment between actin and the membrane, and using the low deformation region of the curve (0−50%), the force deformation (F-ε) follows a simple relationship as expressed in eq 1 below, where E_m is the Young's modulus of the membrane and ν_m represents the Poisson's ratio of the membrane; h is the membrane thickness, R_0 is the radius of the uncompressed cell, and ε is the relative deformation of the cell. The Poisson's ratio is $\nu_m = 1/2$ for living cells whose membrane remains impermeable during the measurements. Cell radius R_0 is determined by the height difference between probe−cell contact and the surface, and the membrane thickness of the membrane is h = 4 nm for the membranes of lipid bilayers. Least square fitting of force-deformation profiles allows for quantification of membrane (E_m) Young's modulus.

$$F_m = 2\pi \frac{E_m}{1-\nu_m} h R_0 \varepsilon^3 \quad (1)$$

Simple geometry was used to calculate the area of the cell surface affected by an incompletely engulfed AgNW. The affected area was calculated using the formula for the area of a circle, $A = \pi r^2$, where A is the affected area, and r is the radius of the AgNW. To calculate the total cell surface area, the cell was assumed to be a sphere that is missing a cap, which accounts for the part of the cell sitting on the surface. The total cell surface area was calculated using the equation below, where S_t is the total surface area of the cell, R is the radius of the cell, and r is the radius of the contact patch.

$$S_t = \pi(4R^2 - (R - \sqrt{R^2 - r^2})^2) \quad (2)$$

RESULTS AND DISCUSSION

Characterization of Ag Nanowires. Prior to exposing cells to nanomaterials, the Ag nanowires were first characterized using AFM. Figure 1 shows AgNWs immobilized on a PLL-coated mica (0001) surface. These immobilized AgNWs

https://dx.doi.org/10.1021/acs.jpcb.0c08132
J. Phys. Chem. B 2020, 124, 11584−11592

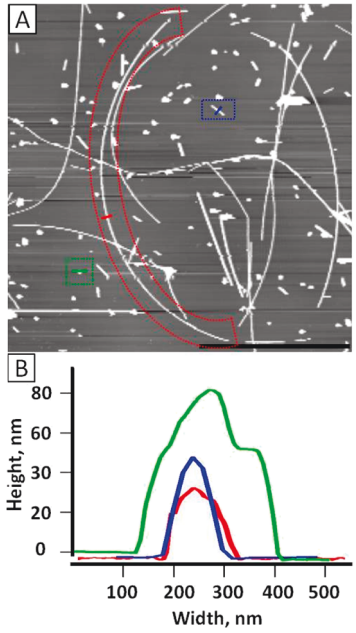

Figure 1. AFM characterization of AgNWs. (A) 23 μm × 23 μm AFM topograph of the AgNWs upon immobilization on a PLL-coated mica (0001) surface. Scale bar = 10 μm. Outlined in red is a typical long AgNW, which is 28 μm long. Blue outline is a typical short AgNW, which is 1.05 μm long. Green outline is a typical Ag nanoparticle (AgNP). (B) Cursor profiles as indicated in (A) with red, blue, and green lines representing the three populations, long wire, short wire, and nanoparticles, respectively.

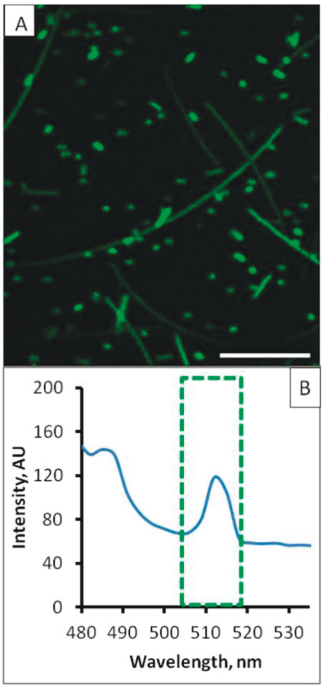

Figure 2. (A) Laser scanning confocal image of the immobilized AgNWs taken under a 458 nm excitation with fluorescence collected within 500−600 nm. Scale bar = 10 μm. (B) Corresponding photoluminescence spectrum, where the emission peak at 515 nm (green enclosure) is responsible for the green color under a 458 nm excitation.

are well separated, and individual wires are clearly visualized. From the topographic image shown in Figure 1A, the AgNWs exhibit a wide distribution in terms of geometry and size. Three types of populations are clearly visible: long wires (5−30 μm), short wires (1−5 μm), and particles (<1 μm). The three enclosures shown in Figure 1A provide representative examples. A long wire (red enclosure) measures 28 μm long and 35.5 nm in diameter, as seen from the cursor profiles in Figure 1B. A short wire (blue enclosure) is 1.05 μm long and 50 nm in diameter (Figure 1B), and a nanoparticle (green enclosure) has the diameter of 85 nm (Figure 1B). Figure 1A is a crop of a larger scan area, 2500 μm^2 in size. In that area, 397 Ag nanostructures were counted. Among them, there were 61 long wires (15.4%), 71 short wires (17.9%), and 265 nanoparticles (66.7%). Additionally, SEM imaging was also acquired to provide another measurement of the population distribution, and the results were consistent with that measured from Figure 1A. EDS was carried out to verify the presence of Ag in the wires, and the 2.984 KeV peak, characteristic of Ag, was clearly visible in the spectra.

Laser scanning confocal microscopy was also carried out for AgNWs upon immobilization on a PLL-coated glass slide. As shown in Figure 2A, these PVP-coated AgNWs exhibit photoluminescent behavior, with fluorescence collected within 500−600 nm. Fluorescence intensity versus the wavelength spectrum with 4 nm increment was also acquired at 458 nm (argon laser) excitation. From the fluorescence spectrum of AgNWs shown in Figure 2B, two emission peaks at 485 and 515 nm are evident. The presence of photoluminescence at 515 nm enables in situ visualization of the precise locations of AgNWs with respect to the living cells during their interactions.

Direct Observations of Frustrated Phagocytosis In Situ. NR8383 cells were placed onto the glass-bottom of the MatTek dishes containing 3 mL of cell culture media; then, 30 μL of 100 μg/mL solution of AgNWs was added to reach the final concentration of 1 μg/mL AgNWs. Then, the dishes were incubated for 24 h in an incubator (37 °C and 5% CO_2). By allowing 24 h interactions, we increased the chance to capture frustrated phagocytosis as the event was known to occur 4 h after exposure.[19] Next, the dishes containing unfixed live NR8383 cells were imaged using combined bright field (BF) and laser scanning confocal microscopy. Figure 3 shows a representative example where frustrated phagocytosis was captured after mixing NR8383 cells with 1 μg/mL AgNWs for 24 h. Figure 3A is a bright field optical microscopy image of a representative NR8383, a D = 12 μm cellular body with multiple filopodia. This morphology is consistent with that of

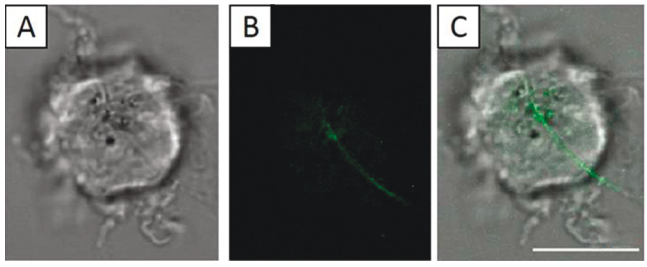

Figure 3. NR8383 cell (living and in culture media) after 24 h exposure in a 1 μg/mL AgNW solution. Scale bar is 10 μm. (A) BF image of the NR8383 cell. (B) Confocal image acquired at 1.96 μm above the glass−cell interface. (C) Overlay of (A) and (B), revealing a long AgNW partially internalized by the cell.

https://dx.doi.org/10.1021/acs.jpcb.0c08132
J. Phys. Chem. B 2020, 124, 11584−11592

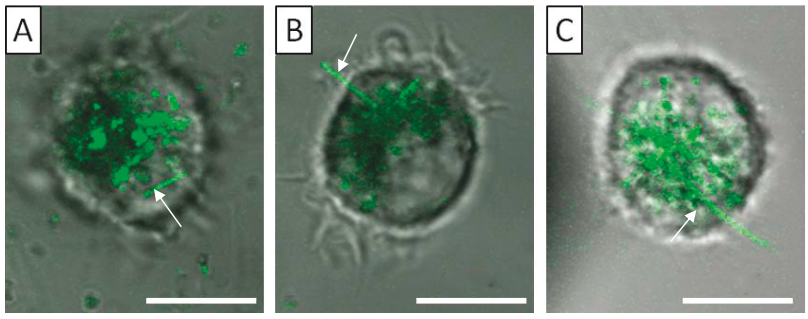

Figure 4. Confocal images overlaid with bright field optical images for three representative NR8383 cells after exposing the set of the cells to 10 μg/mL AgNWs for 24 h. Scale bar is 10 μm. (A) Confocal slice taken at 1.5 μm above the cell−glass interface. The arrow clearly points to a fully engulfed AgNW. (B) Single confocal slice acquired at 8 μm above the cell−glass interface. The arrow indicates a partially internalized AgNW, 6.1 μm long. (C) Single confocal slice acquired at 9 μm above the cell−glass interface. The arrow points to a partially internalized AgNW, 19.7 μm long.

known healthy NR8383 cells.[22,35,36] The confocal imaging was acquired slice-by-slice from the glass−cell interface upward at 280 nm increment, from which the height of the cell was measured as 14.5 μm. Figure 3B represents a single confocal slice starting at 1.96 μm above the glass cover slip. A 19.5 μm-long AgNW was clearly visible. Combined display of Figure 3A,B is shown in Figure 3C, revealing the location of the long AgNW with respect to the cell; 12 μm inside and 7.5 μm outside. The intracellular portion of the wire appears to be mostly in plane of the confocal slice, while the extracellular portion curves at approximately 69° from the surface normal. In contrast to the long AgNW that is partially internalized, multiple short AgNWs and AgNPs were completely taken in by the cell (see the green contrast inside the cell in Figure 3B). Among four sets of experiments carried out under the same conditions as those in Figure 3, and over 30 cells subjected to the detailed confocal and bright field optical imaging, three cases of frustrated phagocytosis occurred. In our attempts to verify the robustness of the observed frustrated phagocytosis, the AgNW concentration was increased to 10 μg/mL. At this concentration, four sets of experiments were carried out, and 14 out of 30 NR8383 cells exhibited partially internalized AgNWs after 24 h exposure. Clearly, the probability for frustrated phagocytosis increased with increasing AgNW concentration.

In order to determine length threshold, the length of AgNWs was measured for all 226 cases of frustrated phagocytosis in this investigation. For each cell, we also measured the longest AgNWs that were fully engulfed. Three regions became clear. AgNWs longer than 15 μm caused frustrated phagocytosis upon interactions with NR8383 cells, while wires shorter than 5 μm were fully engulfed. The transient region includes AgNWs ranging from 5−15 μm, in which full and partial internalizations were both observed. Three representative examples are shown in Figure 4 to illustrate our findings. In the NR8383 cell shown in Figure 4A, a large amount of AgNWs was engulfed (green contrast). We measured the lengths of the fully engulfed AgNWs, the longest being 4.2 μm (as indicated by the arrow). In the NR8383 cell imaged in Figure 4B, a AgNW, 6.1 μm long, was partially internalized. Figure 4C shows an NR8383 cell with a 19.7 μm long AgNW, clearly exhibiting frustrated phagocytosis. Our findings are consistent with prior studies of nanowire-induced frustrated phagocytosis, where the threshold length of frustrated phagocytosis for AgNWs was 14 and 10 μm for THP-1 and mouse lung alveolar macrophages, respectively, as determined from SEM imaging of fixed cells.[19]

While frustrated phagocytosis was captured among living cells for silicon nanowires[37] and CNTs,[38] our results represent the first direct observations of AgNW-induced frustrated phagocytosis in situ and among living cells, to the best of our knowledge.

Cytoskeleton Structural Changes as Results of Nanowire-Induced Frustrated Phagocytosis. In conventional frustrated phagocytosis, when the phagocyte attempts and fails to internalize a microwire, the cell would begin with pseudopod extension, as mediated by actin filaments near the interface. The pseudopod matures into a phagocytic cup, creating a tight seal at the end of the pseudopod, partially surrounding the object being internalized.[39,40] The seal has been recently shown to be an extremely actin-rich cuff, in contrast to the rest of the pseudopod and often the rest of the cell cortex.[40] Given the much smaller diameter of AgNWs (40 nm in our study), it becomes a fundamental question if frustrated phagocytosis of nanowires follows similar behavior. To address this question, we transfected NR8383 cells with Lifeact-TagRFP, which induced cells to express an actin-binding fluorescent tag. These transfected cells, referred to as NR8383-RFP, allowed clear visualization of the cytoskeleton evolution live and in situ. After incubation with 10 μg/mL AgNW in the cell culture media for 24 h, live cells were imaged using LSCM following similar protocols as that in Figure 3. Among 11 sets of experiments and 74 NR8383-RFP cells examined, 63 cells participated in frustrated phagocytosis.

Since RFP and AgNWs exhibit different fluorescence spectra, it is easy to capture both at the same time using confocal imaging; under 458 nm excitation, AgNWs emit at 500−520 nm (Figure 2), while RFP exhibits emission at 595−665 nm under 543 nm excitation. Figure 5 shows two AgNWs causing frustrated phagocytosis in a NR8383-RFP cell. One of the AgNWs was 20 μm long (arrow 1), which clearly crossed the cellular membrane and actin cortex of the NR8383-RFP cell, with 4 μm of the total length inside the cell. This AgNW was inclined at 81.9° from the surface normal. At the entry site, actin wrapped the external portion of the AgNW, extending out to 8 μm from the actin cortex. The other AgNW (arrow 2) was 18 μm long and was inclined at 80.4° from the surface normal. Its proximal end appeared to have reached the main actin cortex. Similar to the first AgNW, the actin protrusion extended 8 μm from the main actin cortex, wrapping around

https://dx.doi.org/10.1021/acs.jpcb.0c08132
J. Phys. Chem. B 2020, 124, 11584−11592

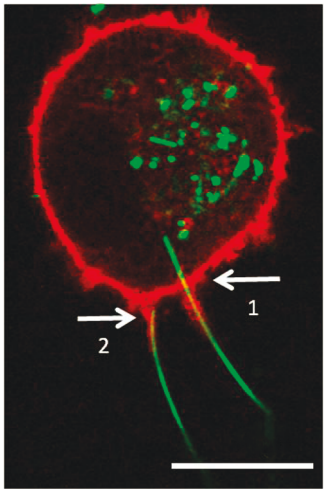

Figure 5. NR8383-RFP cell exposed to 10 μg/mL AgNWs for 24 h. The confocal images were acquired at 1.2 μm above the cell−glass interface, by overlaying the AgNW (green) and RFP (tagging actin) fluorescence (red) images. Arrow 1 points to a partially internalized AgNW. Arrow 2 points to another AgNW whose end just reached the cell's actin cortex. Scale bar is 10 μm.

the AgNW, and appeared to have been pulling the AgNW into the cell.

Actin density, as observed by the intensity of the RFP, was stronger in the actin cortex than in the pseudopods wrapping around the AgNWs. The actin distribution inside the pseudopod was observed to be roughly homogeneous from its end all the way to its base. As mentioned earlier, frustrated phagocytosis of microfibers involves the pseudopod growth and formation of highly actin-enriched cuff at the distal end of the pseudopod, 3−5 μm in width.[40] The highly actin-enriched cuff appears to be conserved among many cell types, as it was also observed during frustrated phagocytosis in *Dictyostelium discoideum*,[41] and during normal phagocytosis in NR8383 cells.[42] The high concentration of actin at the entry sight was similarly shown for frustrated phagocytosis of microscale bundles of polymer nanofibers, along with intracellular actin accumulation around the incompletely engulfed bundles.[18] In contrast, the AgNW-induced frustrated phagocytosis significantly differs. In the case of AgNWs, a tight actin is wrapped along the pseudopods from the base to the end, with only minor enrichment occurring closer to the cortex. The fact that the cortex and the pseudopod have similar concentrations of actin represents another indication that the local structural perturbations at entry sites caused by AgNWs appeared to be smaller than that of the microwires. In contrast, the cytoskeleton actin "climbed up" along the nanowire in the case of AgNW-induced frustrated phagocytosis. This observation suggests that the actin remodeling during nanowire-initiated frustrated phagocytosis is unique to nanomaterials and certainly warrants further investigation.

Occasionally, multiple cells in neighboring positions participated in frustrated phagocytosis with multiple AgNWs. In Figure 6, four NR8383-RFP cells are arranged approximately linearly, as seen from both the confocal image taken at 7.4 μm above the glass−cell interface (Figure 6A) and the bright field optical image (Figure 6B). The two adjacent cells were "linked" via AgNWs, each having internalized a portion of the AgNWs, analogous to the concept of a skewer. The partial internalization between adjacent cells represents another situation of frustrated phagocytosis, referred to by us as cellular aggregation via frustrated phagocytosis. A single AgNW is shown involved at the first joint (arrow 1). The AgNW is visible crossing from the first to the second cell, pointed at by the white triangles. Similar behavior is shown at joints 2 and 3. In these cases, the wires appeared bundled as they present crossing from cell to cell. As indicated in previous sections, AgNWs remained dispersed as individual entities in the solution and media: thus, the bundling and alignment were the results of AgNW−cell interactions. These AgNWs appeared as yellow contrast (see sites indicated by the three arrows), as a result of the superposition of the AgNWs (green) and the RFP-actin (red) fluorescence. This observation is consistent with our earlier conclusions that AgNWs are wrapped by actin at frustrated phagocytosis sites. The actin was likely the structural support to the cellular membrane, creating partial wrapping of the AgNWs. In contrast to the situation observed in Figure 5, Figure 6 revealed accumulation of red fluorescence at the cytoskeleton near the nanowire entry, suggesting the enrichment of actin, in the case of cellular aggregation via frustrated phagocytosis. In the 11 sets of experiments, i.e., 74 NR8383-RFP cells examined, 63 cells participated in frustrated phagocytosis among which eight

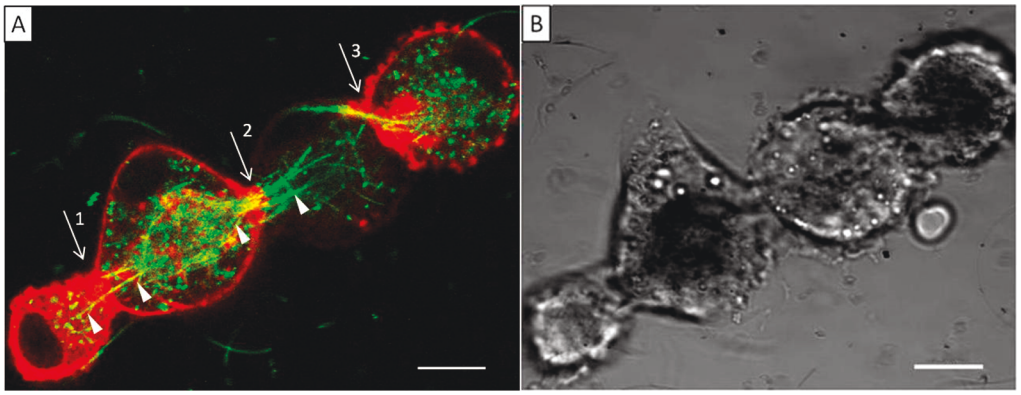

Figure 6. (A) Single confocal slice taken at 7.4 μm above the cell−glass interface, displayed by overlaying the AgNW (green) and RFP-actin (red) fluorescence images. Arrows point to the cellular entry sites where frustrated phagocytosis occurred. White triangles point at AgNWs that clearly cross from one cell to another. The degree of transfection varied from cell to cell (e.g., the third cell has lower transfection than others). (B) Bright field optical image taken at the same time over the same region. Scale bar is 10 μm.

https://dx.doi.org/10.1021/acs.jpcb.0c08132
J. Phys. Chem. B 2020, 124, 11584−11592

cellular aggregates (2−8 cells) were observed. Macrophage aggregation around microwires[43] and nanowires[14] has been previously observed using bright field microscopy of fixed cells. Here, we show evidence of frustrated phagocytosis-driven aggregation in live cells, resulting in a "skewered" geometry. The observation is significant to our understanding of the impact of nanowire−macrophage interactions and potential toxicity downstream. Macrophages typically form an aggregate, when individual macrophages cannot remove the foreign material.[44] Such aggregates are likely to lead to reduced AgNW clearance in the lungs, since macrophages need to migrate to bronchioles in order to be picked up by the mucociliary escalator.[44,45] Bulk macrophage motility assays have previously shown a strong positive correlation between AgNW length and reduction in motile function.[15] This linear macrophage aggregation due to long AgNWs could be one of the reasons for reduced motility. If left in this state for a prolonged period of time, this type of macrophage aggregation is likely to result in formation of foreign body giant cells,[14] which tend to form if foreign materials cannot be removed in two to four weeks.[46]

Probing the Impact of AgNW-Induced Frustrated Phagocytosis on Cellular Mechanical Properties. It is known that conventional frustrated phagocytosis causes significant changes to the cellular membrane and cytoskeleton, especially at the entry sites.[40,47] These structural changes are expected to alter the cellular mechanical properties. Due to the ultrasmall diameter and high aspect ratio, nanowire leads to structural changes different from that in conventional frustrated phagocytosis, as discussed in previous sections. Therefore, this section investigates whether the cellular mechanics would change due to AgNW-induced frustrated phagocytosis.

Our prior work (see also the Introduction and Methods sections) has indicated that single cell compression (SSC) provides a sensitive and accurate means to assess the mechanical properties of the membrane and cytoskeleton qualitatively and quantitatively at a single cell level.[9,20,21,48] In addition, all SCC measurements could be taken in culture media and under incubation conditions to preserve the integrity of the cellular biostatus.[49] To tease out the impact of frustrated phagocytosis of AgNWs, with minimal interference by Ag nanoparticles and short wires in the mixture, we utilized a low concentration of AgNWs, 1 μg/mL, and 24 h incubation. Additionally, NR8383 cells with a single event of AgNW phagocytosis, and minimal intake of Ag nanoparticles, were selected to be probed by SCC.

Figure 7 compares the force-deformation profiles of a control (black) versus a NR8383 cell undergoing frustrated phagocytosis (blue). The two profiles appear to be very similar. It took 22.3 and 88.1 nN of normal force to compress the NR8383 cell undergoing frustrated phagocytosis to 30 and 60% deformation, respectively, while the forces measured as 14.2 and 96.6 nN are for that of the control cell. Among all cells subject to SCC measurements, 30 and 60% deformation required forces of 20.3−33.5 nN and 88.1−139.1 nN, respectively, for cells undergoing frustrated phagocytosis. The forces required were 6.3−29.0 nN and 69.6−139.0 nN, respectively, for that of cells without AgNW exposure. Therefore, NR8383 cells remain viable based on the morphology (see optical microscopy images) and force profiles. A dead cell would exhibit softer mechanics due to damage to the membrane, based on our prior work[20] and work by others.[50] The similarity of force-deformation profiles

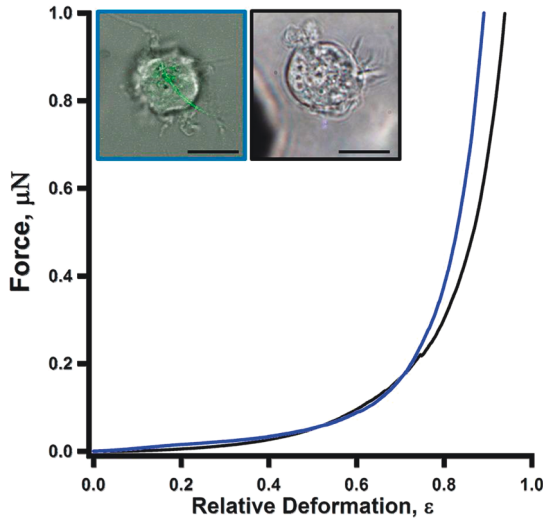

Figure 7. Force versus relative deformation measurements for the two presentative NR8383 cells. All scale bars in the inset images are 10 μm. Left inset: a bright field optical image overlaid with a confocal slice acquired at 6.72 μm above the cell−glass interface. Right inset: a bright field optical microscopy image only. A NR8383 cell (blue curve) after exposure to 1 μg/mL AgNWs for 24 h was undergoing frustrated phagocytosis induced by a 19.5 μm-long AgNW (left image). Another NR8383 cell (black curve) without exposure to AgNWs (right image).

suggests that a single AgNW-induced frustrated phagocytosis had little impact on the overall cellular mechanics.

Least square fitting of the F-ε profiles shown in Figure 7 using eq 1 yielded Young's modulus of the membrane (E_m) as 1.38 and 1.31 MPa for the cells with and without AgNW exposure, respectively. Among all cells investigated, the Young's modulus E_m ranged from 1.38−1.95 MPa for NR8383 cells undergoing a single AgNW-induced frustrated phagocytosis, while unexposed cells were ranged from 0.79−1.71 MPa. The membrane Young's modulus measured for NR8383 cells appears to be similar to that of other phagocytic cell lines, such as BV-2 microglia (E_m = 0.62 ± 0.28 MPa),[49] and softer than MDA-MB-468, a mammary gland cell line (E_m = 1.5−3.1 MPa), and MLC-SV40, a prostatic epithelial cell line (E_m = 1.7−4.9 MPa).[51] These comparisons are rational as NR8383 belong to the phagocytic cell lines. The observed similarity among control and single-wire penetrated cells indicates that the effect of a single AgNW-driven frustrated phagocytosis was localized, and the actin cortex and membrane mechanics at the cellular level did not seem to alter significantly. In a recent work, there was evidence of a possible increase of local stiffness due to frustrated phagocytosis of microscale bundles of polymer nanofibers, which is partially attributed to actin accumulation.[18] In our case, the fact that the mechanical properties of the cell did not significantly change suggests that the structural changes caused by nano-frustrated phagocytosis were very localized to the entry sites. This is consistent with our confocal imaging studies. Since the AgNW diameters ranged from 35 to 85 nm, the immediately affected area of the membrane, and the gap in the continuity of the actin cortex on this cell was between 962 and 5672 nm^2. Using eq 2, the cell surface area was calculated using the approximation of a sphere that is missing a cap. For this cell, whose diameter measured to 14.4 μm, and the cap diameter (surface patch) measured to 6 μm, the total cell membrane

https://dx.doi.org/10.1021/acs.jpcb.0c08132
J. Phys. Chem. B 2020, 124, 11584−11592

area was calculated to be 6.5×10^8 nm^2, which was 5 orders of magnitude larger than that of the AgNW penetrated regions.

CONCLUSIONS

Frustrated phagocytosis has been suspected of and attributed to causing the toxicity of long nanowires. This investigation, using single cell-based methods such as laser scanning confocal microscopy and single cell mechanics, captured frustrated phagocytosis of long AgNWs in their entry into NR8383 cells. Frustrated phagocytosis was observed at AgNW concentrations as low as 1 μg/mL after 24 h of exposure. Tagging cytoskeleton actin with RFP, we were able to reveal the role of actin. At the frustrated phagocytosis site, actin wrapped around the AgNWs extruding away from the membrane, as far as 8 μm, i.e., forming pseudopods. From our SCC measurements, the single wire-induced frustrated phagocytosis did not exhibit significant impact to the overall cellular mechanical properties, which is consistent with confocal imaging revealing actin changes remained localized at the entry sites. In some cases of frustrated phagocytosis, NR8383 aggregation happened, where wires connected neighboring cells like a skewer. This observed aggregation is likely to contribute to reduced AgNW clearance from the lungs due to reduced macrophage motility and is probably a precursor to foreign body giant cell formation. Work is in progress to probe further the actin remodeling due to nanowire−cell interaction and to pursue time-dependent investigations of AgNW−cell interactions. This study clearly reveals the unique and characteristic behavior of nanowire-induced frustrated phagocytosis, which deepens our understanding of nanowire−cell interactions and nanocytotoxicity.

AUTHOR INFORMATION

Corresponding Author

Gang-yu Liu − *Biophysics Graduate Group and Department of Chemistry, University of California, Davis, California 95616, United States;* orcid.org/0000-0003-3689-0685; Phone: (530) 754-9678; Email: gyliu@ucdavis.edu; Fax: (530) 752-8995

Authors

Evgeny Ogorodnik − *Biophysics Graduate Group, University of California, Davis, California 95616, United States*

Arpad Karsai − *Department of Chemistry, University of California, Davis, California 95616, United States*

Kang-Hsin Wang − *Department of Dermatology, University of California Davis, School of Medicine, Sacramento, California 95817, United States*

Fu-tong Liu − *Institute of Biomedical Sciences, Academia Sinica, Taipei 11529, Taiwan*

Su Hao Lo − *Department of Biochemistry and Molecular Medicine, University of California Davis, Sacramento, California 95817, United States*

Kent E. Pinkerton − *Department of Pediatrics, University of California Davis, School of Medicine, Sacramento, California 95817, United States*

Benjamin Gilbert − *Energy Geoscience Division, Lawrence Berkeley National Laboratory, Berkeley, California 94720, United States;* orcid.org/0000-0003-0853-0826

Dominik R. Haudenschild − *Department of Orthopedic Surgery, University of California Davis Medical Center, Sacramento, California 95817, United States*

Complete contact information is available at: https://pubs.acs.org/10.1021/acs.jpcb.0c08132

Notes

The authors declare no competing financial interest.

ACKNOWLEDGMENTS

We thank Ms. Victoria Tran for her technical assistance in SEM and EDS measurements. This work was supported by the UC Davis, the National Institutes of Health (R01-AR070239), the W.M. Keck Foundation, the National Science Foundation (CHE-1808829), the National Institute of Environmental Health Sciences (U01-ES027288), the Gordon and Betty Moore Foundation, and partly supported by DOE BES under Contract DE-AC02-05CH11231.

REFERENCES

(1) Wu, S.; Peng, S.; Yu, Y.; Wang, C.-H. Strategies for Designing Stretchable Strain Sensors and Conductors. *Adv. Mater. Technol.* **2020**, *5*, 1900908.

(2) Moon, H.; Won, P.; Lee, J.; Ko, S. H. Low-haze, annealing-free, very long Ag nanowire synthesis and its application in a flexible transparent touch panel. *Nanotechnology* **2016**, *27*, 295201.

(3) Jung, J.; Cho, H.; Yuksel, R.; Kim, D.; Lee, H.; Kwon, J.; Lee, P.; Yeo, J.; Hong, S.; Unalan, H. E.; et al. Stretchable/flexible silver nanowire electrodes for energy device applications. *Nanoscale* **2019**, *11*, 20356.

(4) Jiang, S.; Teng, C. P. Fabrication of silver nanowires-loaded polydimethylsiloxane film with antimicrobial activities and cell compatibility. *Mater. Sci. Eng., C* **2017**, *70*, 1011.

(5) Park, J.; Kwak, B. K.; Bae, E.; Lee, J.; Kim, Y.; Choi, K.; Yi, J. Characterization of exposure to silver nanoparticles in a manufacturing facility. *J. Nanopart. Res.* **2009**, *11*, 1705.

(6) Theodorou, I.; Ryan, M.; Tetley, T.; Porter, A. Inhalation of silver nanomaterials–seeing the risks. *Int. J. Mol. Sci.* **2014**, *15*, 23936.

(7) Verma, N. K.; Conroy, J.; Lyons, P. E.; Coleman, J.; O'Sullivan, M. P.; Kornfeld, H.; Kelleher, D.; Volkov, Y. Autophagy induction by silver nanowires: a new aspect in the biocompatibility assessment of nanocomposite thin films. *Toxicol. Appl. Pharmacol.* **2012**, *264*, 451.

(8) Fubini, B.; Fenoglio, I.; Tomatis, M.; Turci, F. Effect of chemical composition and state of the surface on the toxic response to high aspect ratio nanomaterials. *Nanomedicine* **2011**, *6*, 899.

(9) Liu, Y. X.; Karsai, A.; Anderson, D. S.; Silva, R. M.; Uyeminami, D. L.; Van Winkle, L. S.; Pinkerton, K. E.; Liu, G. Y. Single-Cell Mechanics Provides an Effective Means To Probe in Vivo Interactions between Alveolar Macrophages and Silver Nanoparticles. *J. Phys. Chem. B* **2015**, *119*, 15118.

(10) Jia, M.; Zhang, W.; He, T.; Shu, M.; Deng, J.; Wang, J.; Li, W.; Bai, J.; Lin, Q.; Luo, F.; et al. Evaluation of the Genotoxic and Oxidative Damage Potential of Silver Nanoparticles in Human NCM460 and HCT116 Cells. *Int. J. Mol. Sci.* **2020**, *21*, 1618.

(11) Barkur, S.; Lukose, J.; Chidangil, S. Probing Nanoparticle-Cell Interaction Using Micro-Raman Spectroscopy: Silver and Gold Nanoparticle-Induced Stress Effects on Optically Trapped Live Red Blood Cells. *ACS Omega* **2020**, *5*, 1439.

(12) Wang, F.; Wang, Y.; Yao, X.; Ma, C.; Yin, Y.; Song, M. Length and diameter-dependent phagocytosis and cytotoxicity of long silver nanowires in macrophages. *Chemosphere* **2019**, *237*, 124565.

(13) Lehmann, S. G.; Toybou, D.; Pradas Del Real, A. E.; Arndt, D.; Tagmount, A.; Viau, M.; Safi, M.; Pacureanu, A.; Cloetens, P.; Bohic, S.; et al. Crumpling of silver nanowires by endolysosomes strongly reduces toxicity. *Proc. Natl. Acad. Sci. U. S. A.* **2019**, *116*, 14893.

(14) Silva, R. M.; Xu, J.; Saiki, C.; Anderson, D. S.; Franzi, L. M.; Vulpe, C. D.; Gilbert, B.; Van Winkle, L. S.; Pinkerton, K. E. Short versus long silver nanowires: a comparison of in vivo pulmonary effects post instillation. *Part. Fibre Toxicol.* **2014**, *11*, 52.

(15) Schinwald, A.; Chernova, T.; Donaldson, K. Use of silver nanowires to determine thresholds for fibre length-dependent pulmonary inflammation and inhibition of macrophage migration in vitro. *Part. Fibre Toxicol.* **2012**, *9*, 47.

(16) Donaldson, K.; Murphy, F. A.; Duffin, R.; Poland, C. A. Asbestos, carbon nanotubes and the pleural mesothelium: a review of the hypothesis regarding the role of long fibre retention in the parietal pleura, inflammation and mesothelioma. *Part. Fibre Toxicol.* **2010**, *7*, 5.
(17) Ishida, T.; Fujihara, N.; Nishimura, T.; Funabashi, H.; Hirota, R.; Ikeda, T.; Kuroda, A. Live-cell imaging of macrophage phagocytosis of asbestos fibers under fluorescence microscopy. *Genes Environ.* **2019**, *41*, 14.
(18) Zhou, G.; Zhang, B.; Wei, L.; Zhang, H.; Galluzzi, M.; Li, J. Spatially Resolved Correlation between Stiffness Increase and Actin Aggregation around Nanofibers Internalized in Living Macrophages. *Materials* **2020**, *13*, 3235.
(19) Schinwald, A.; Donaldson, K. Use of back-scatter electron signals to visualise cell/nanowires interactions in vitro and in vivo; frustrated phagocytosis of long fibres in macrophages and compartmentalisation in mesothelial cells in vivo. *Part. Fibre Toxicol.* **2012**, *9*, 34.
(20) Lulevich, V.; Zink, T.; Chen, H.-Y.; Liu, F.-T.; Liu, G.-Y. Cell mechanics using atomic force microscopy-based single-cell compression. *Langmuir* **2006**, *22*, 8151.
(21) Lulevich, V.; Zimmer, C. C.; Hong, H.-S.; Jin, L.-W.; Liu, G.-Y. Single-cell mechanics provides a sensitive and quantitative means for probing amyloid-beta peptide and neuronal cell interactions. *Proc. Natl. Acad. Sci. U. S. A.* **2010**, *107*, 13872.
(22) Helmke, R. J.; Boyd, R. L.; German, V. F.; Mangos, J. A. From Growth Factor Dependence to Growth Factor Responsiveness: the Genesis of an Alveolar Macrophage Cell Line. *In Vitro Cell. Dev. Biol.* **1987**, *23*, 567.
(23) Helmke, R. J.; German, V. F.; Mangos, J. A. A continuous alveolar macrophage cell line: comparisons with freshly derived alveolar macrophages. *In Vitro Cell. Dev. Biol.* **1989**, *25*, 44.
(24) Griscavage, J. M.; Rogers, N. E.; Sherman, M. P.; Ignarro, L. J. Inducible nitric oxide synthase from a rat alveolar macrophage cell line is inhibited by nitric oxide. *J. Immunol.* **1993**, *151*, 6329.
(25) Hidalgo, H. A.; Helmke, R. J.; German, V. F.; Mangos, J. A. Pneumocystis carinii induces an oxidative burst in alveolar macrophages. *Infect. Immun.* **1992**, *60*, 1.
(26) Wiemann, M.; Vennemann, A.; Wohlleben, W. Lung Toxicity Analysis of Nano-Sized Kaolin and Bentonite: Missing Indications for a Common Grouping. *Nanomaterials* **2020**, *10*, 204.
(27) Bannuscher, A.; Karkossa, I.; Buhs, S.; Nollau, P.; Kettler, K.; Balas, M.; Dinischiotu, A.; Hellack, B.; Wiemann, M.; Luch, A.; et al. A multi-omics approach reveals mechanisms of nanomaterial toxicity and structure-activity relationships in alveolar macrophages. *Nanotoxicology* **2020**, *14*, 181.
(28) Wiemann, M.; Sauer, U.; Vennemann, A.; Bäcker, S.; Keller, J.-G.; Ma-Hock, L.; Wohlleben, W.; Landsiedel, R. In Vitro and In Vivo Short-Term Pulmonary Toxicity of Differently Sized Colloidal Amorphous SiO_2. *Nanomaterials* **2018**, *8*, 160.
(29) ATCC. Product Sheet NR8383 [AgC11x3A, NR8383.1] (ATCC® CRL2192™). https://www.atcc.org/~/ps/CRL-2192.ashx (accessed 02.25.2020).
(30) Quiagen *Effectene® Transfection Reagent Handbook*; Quiagen: 2002.
(31) Burgess, A.; Vigneron, S.; Brioudes, E.; Labbé, J.-C.; Lorca, T.; Castro, A. Loss of human Greatwall results in G2 arrest and multiple mitotic defects due to deregulation of the cyclin B-Cdc2/PP2A balance. *Proc. Natl. Acad. Sci. U. S. A.* **2010**, *107*, 12564.
(32) Deng, Z.; Zink, T.; Chen, H. Y.; Walters, D.; Liu, F. T.; Liu, G. Y. Impact of actin rearrangement and degranulation on the membrane structure of primary mast cells: a combined atomic force and laser scanning confocal microscopy investigation. *Biophys. J.* **2009**, *96*, 1629.
(33) Cleveland, J. P.; Manne, S.; Bocek, D.; Hansma, P. K. A Nondestructive Method for Determining the Spring Constant of Cantilevers for Scanning Force Microscopy. *Rev. Sci. Instrum.* **1993**, *64*, 403.
(34) Sader, J. E.; Larson, I.; Mulvaney, P.; White, L. R. Method for the Calibration of Atomic-Force Microscope Cantilevers. *Rev. Sci. Instrum.* **1995**, *66*, 3789.
(35) Xu, L.; Dai, Y.; Wang, Z.; Zhao, J.; Li, F.; White, J. C.; Xing, B. Graphene quantum dots in alveolar macrophage: uptake-exocytosis, accumulation in nuclei, nuclear responses and DNA cleavage. *Part. Fibre Toxicol.* **2018**, *15*, 45.
(36) ATCC. https://www.atcc.org/~/media/Attachments/Micrographs/Cell/CRL-2192.ashx (accessed 03.15.2020).
(37) Zimmerman, J. F.; Parameswaran, R.; Murray, G.; Wang, Y.; Burke, M.; Tian, B. Cellular uptake and dynamics of unlabeled freestanding silicon nanowires. *Sci. Adv.* **2016**, *2*, No. e1601039.
(38) Boyles, M. S. P.; Young, L.; Brown, D. M.; MacCalman, L.; Cowie, H.; Moisala, A.; Smail, F.; Smith, P. J. W.; Proudfoot, L.; Windle, A. H.; et al. Multi-walled carbon nanotube induced frustrated phagocytosis, cytotoxicity and pro-inflammatory conditions in macrophages are length dependent and greater than that of asbestos. *Toxicol. In Vitro* **2015**, *29*, 1513.
(39) Wright, S. D.; Silverstein, S. C. Phagocytosing macrophages exclude proteins from the zones of contact with opsonized targets. *Nature* **1984**, *309*, 359.
(40) Maxson, M. E.; Naj, X.; O'Meara, T. R.; Plumb, J. D.; Cowen, L. E.; Grinstein, S. Integrin-based diffusion barrier separates membrane domains enabling the formation of microbiostatic frustrated phagosomes. *eLife* **2018**, *7*, No. e34798.
(41) Gerisch, G.; Ecke, M.; Schroth-Diez, B.; Gerwig, S.; Engel, U.; Maddera, L.; Clarke, M. Self-organizing actin waves as planar phagocytic cup structures. *Cell Adhes. Migr.* **2009**, *3*, 373.
(42) Champion, J. A.; Mitragotri, S. Role of target geometry in phagocytosis. *Proc. Natl. Acad. Sci. U. S. A.* **2006**, *103*, 4930.
(43) Lee, J. M.; Kim, Y. J. Foreign body granulomas after the use of dermal fillers: pathophysiology, clinical appearance, histologic features, and treatment. *Arch. Plast. Surg.* **2015**, *42*, 232.
(44) Pagán, A. J.; Ramakrishnan, L. The Formation and Function of Granulomas. *Annu. Rev. Immunol.* **2018**, *36*, 639.
(45) Green, G. M.; Jakab, G. J.; Low, R. B.; Davis, G. S. Defense mechanisms of the respiratory membrane. *Am. Rev. Respir. Dis.* **1977**, *115*, 479.
(46) Chen, S.; Jones, J. A.; Xu, Y.; Low, H. Y.; Anderson, J. M.; Leong, K. W. Characterization of topographical effects on macrophage behavior in a foreign body response model. *Biomaterials* **2010**, *31*, 3479.
(47) Takemura, R.; Stenberg, P. E.; Bainton, D. F.; Werb, Z. Rapid redistribution of clathrin onto macrophage plasma membranes in response to Fc receptor-ligand interaction during frustrated phagocytosis. *J. Cell Biol.* **1986**, *102*, 55.
(48) Zimmer, C. C.; Liu, Y. X.; Morgan, J. T.; Yang, G.; Wang, K. H.; Kennedy, I. M.; Barakat, A. I.; Liu, G. Y. New approach to investigate the cytotoxicity of nanomaterials using single cell mechanics. *J. Phys. Chem. B* **2014**, *118*, 1246.
(49) Liu, Y. X. *A New Approach for Nanotoxicity Assessment: Atomic Force Microscopy based Single Cell Mechanics*. Ph.D. Dissertation. University of California, Davis, 2014.
(50) Nikolaev, N. I.; Müller, T.; Williams, D. J.; Liu, Y. Changes in the stiffness of human mesenchymal stem cells with the progress of cell death as measured by atomic force microscopy. *J. Biomech.* **2014**, *47*, 625.
(51) Lulevich, V.; Shih, Y. P.; Lo, S. H.; Liu, G. Y. Cell tracing dyes significantly change single cell mechanics. *The journal of physical chemistry. B* **2009**, *113*, 6511.

https://dx.doi.org/10.1021/acs.jpcb.0c08132
J. Phys. Chem. B 2020, 124, 11584−11592